



Coulomb effect in hybrid double quantum dot-metal nanoparticle systems considering the wetting layer

Nour A. Nasser^{1,2} and Amin H. Al-Khursan^{1,2*}

*Correspondence:

ameen_2all@yahoo.com

¹Department of Physics, College of Science, University of Thi-Qar, Nasiriya, Iraq

²Nasiriya Nanotechnology Research Laboratory (NNRL), College of Science, University of Thi-Qar, Nasiriya, Iraq

Abstract

Many body effects in the wetting layer (WL)-double quantum dot (DQD)-metal nanoparticle (MNP) structure have been studied by modeling the Coulomb scattering rates in this structure. The strong coupling between WL-DQD-MNPs was considered. An orthogonalized plane wave (OPW) is assumed between WL-QD transitions. The transition momenta are calculated accordingly to specify the normalized Rabi frequency on this structure, considering the strong coupling between the WL-DQD-MNP structures. This approach is important for realizing scattering rates, including in-and-out capture and relaxation rates, which are essential for specifying the type of structure used depending on the optimum value of the scattering time required to fit the application. The QD hole capture rate is the highest, and the hole capture times are the shortest. The relaxation times are less than the electron capture times by one order, while they are half of the hole capture times. The capture rates increase with increasing distance R between the DQDs and the MNP. High tunneling increases hole-capture rates and changes the relaxation rates, showing the importance of tunneling in controlling the scattering rates.

Keywords: Coulomb scattering rates; Metal nanoparticle; Double quantum dot; Capture rate; Relaxation rate; OPW; Wetting layer

1 Introduction

Quantum dot (QD) nanostructures are promising for future devices [1]. The development of nano growth methods has made aligning QDs with metal nanoparticles (MNPs) easy. As strong coupling in MNP-QD systems has been proven, controlling the dynamics and parameters of MNP-QD systems has become desirable [2–4]. The MNP surface plasmonic field and QD excitons interact via Coulomb interactions with energy transfer [5]. The frequency-dependent absorption and scattering, i.e., near-field enhancement, are detected in the strong coupling regime. This enables the spectroscopy of the enhanced surface used in many applications, such as Raman spectroscopy and biochemical sensors [6]. He and Zho [5] studied the strong coupling in a double MNP-QD system via quantum electrodynamics and canonical transformations. The importance of Fano resonance is determined. Trügler and Hohenester used quantum mechanics to describe surface-plasmon-

© The Author(s) 2024. **Open Access** This article is licensed under a Creative Commons Attribution 4.0 International License, which permits use, sharing, adaptation, distribution and reproduction in any medium or format, as long as you give appropriate credit to the original author(s) and the source, provide a link to the Creative Commons licence, and indicate if changes were made. The images or other third party material in this article are included in the article's Creative Commons licence, unless indicated otherwise in a credit line to the material. If material is not included in the article's Creative Commons licence and your intended use is not permitted by statutory regulation or exceeds the permitted use, you will need to obtain permission directly from the copyright holder. To view a copy of this licence, visit <http://creativecommons.org/licenses/by/4.0/>.

polaritons and molecular dynamics and demonstrated strong coupling in an MNP-QD hybrid system [2]. In the quasistatic regime, where the light wavelength is much larger than the MNP size, and the MNP-QD distance, Hohenester and Trügler used the Green function as an essential couple between classical Maxwell and quantum electrodynamics. These methods separate the decay rate into radiative and nonradiative components [6]. Both [2] and [6] use the boundary element approach to calculate the decay rates. Refs. [1, 5, 6] exploit the Drude model to describe the electrons in an MNP.

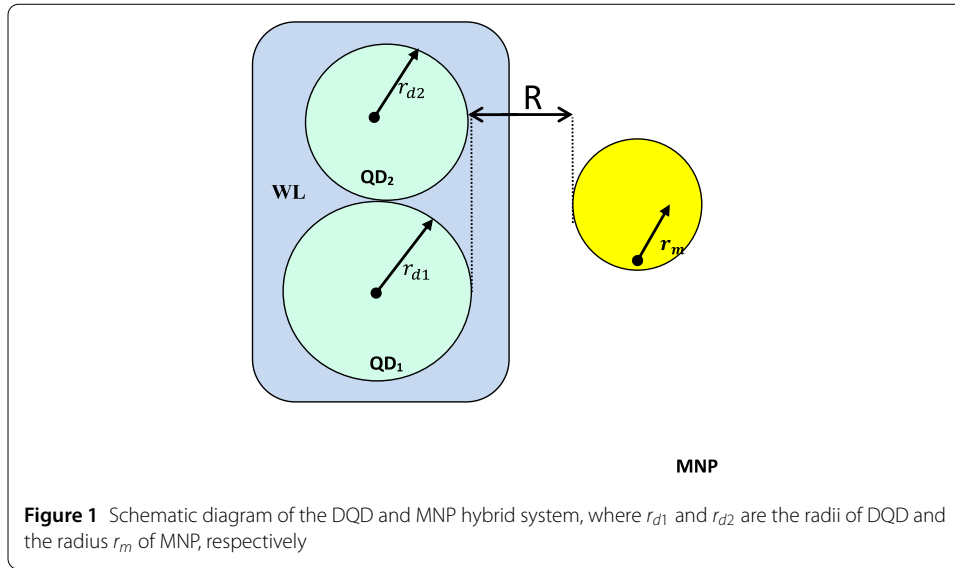
Many-body effects affect the optical properties of QD nanostructure devices. The simple rate equations cannot represent the essential dynamics in a nonequilibrium case [7]. The density matrix theory simulates QD, DQD, and MNP-DQD systems [8]. Such modeling is adequate for describing the interaction between states well through the density element ρ_{ij} , which cannot be calculated with rate equations. Modeling of QD and DQD systems under many-body effects has been performed [9]. However, modeling the many-body effect in MNP-QDs has not been achieved.

The QD nanostructure was grown conventionally on a wetting layer (WL) in Stranaska–Krastanov growth mode (by molecular beam epitaxy). It is an ordinary quantum well (QW) layer, a two-dimensional layer quantized in one dimension (1D). As shown in Fig. 1, carrier transitions from WL to QDs are inevitable in the WL-QD structures. This is because the WL is a reservoir of carriers, and if there is an injection in the device (laser or light emitting diode device), the injection occurs on the WL, and then the carriers can reach the QD state. WL is only quantized in 1D, while QDs are quantized in total (3D). Physically, the transitions occur only between the states of the same quantized numbers. Therefore, transitions between the in-plane (two dimensions) WL and the QDs are impossible. The orthogonalized plane wave (OPW) approximation is required in the WL-QD simulation to satisfy this reality. In OPW, the plane wavefunction of the WL is orthogonalized on the QD state wavefunctions. Then, the transitions occur only between quantized states of the same quantum numbers. This formulation is not easy to apply and is only used in a limited number of works [8, 9]; simplified approximations are employed. Earlier works [10, 11] used OPW and considered the QD wavefunction as a simple harmonic oscillator and the quantum well (QW) WL an infinite structure that oversimplified the problem. However, one must refer to their high work on putting the main points on modeling.

The InAs/GaAs DQD system was detected experimentally by Tarasov et al. [12]. The attachment of QDs to MNPs via bimolecular centers was described in many articles [13, 14]. Zhang et al. clarified the alignment of MNPs to QDs via molecular beam epitaxy through strain-driven nucleation [15]. Therefore, preparing such a hybrid structure was possible.

The WL-DQD-MNP structure was studied in our earlier works [8, 16] by applying the OPW (which has not been involved before in QD-MNP works). However, the Coulomb effect has never been discussed in these works or others dealing with WL-QD-MNPs in the strong coupling case. Each work addresses QD-MNPs or semiconductor nanostructure-MNPs; one can see the direct lines in their sketches, referred to as the Coulomb effect. However, no one has studied this phenomenon, and the real problem of strong coupling (in the case here, where MNP is nearest to QDs) has been approximated and not solved.

This work models the many-body effects in the WL-DQD-MNP structure considering the OPW, which is inevitable in WL-QD transitions. In addition to this modeling, this work has many perspectives. The effect of MNP was evaluated by normalization of the Rabi frequency. The carrier occupation probability is computed through the density ma-



trix theory by modeling the scattering rates. The literature uses experimental data from materials different from those in the understudy or normalized values for energies and momenta. In this work, the WL and QD energies are calculated and subsequently used to estimate the momenta, which calculates the Rabi frequency. The capture rates increase with increasing distance R between the DQDs and the MNP.

The paramount importance of such modeling is to specify the scattering (capture and relaxation) rates. Therefore, one can determine if the scattering is strong (one of the results here is increasing the scattering with MNP-DQD distance). For example, high scattering is required for high-speed frequency modulation. Then, one can desire the structure necessary depending on the needed application. A comparison with the results of other works (with WL-QD structures) provides insight into the correctness of the results obtained here.

2 DQD-MNP structure

The case of study here is the hybrid DQD-MNP structure with DQDs of two InAs QDs, a quantum disk shape, each with r_{d1} ($= 13 \text{ nm}$) and r_{d2} ($= 11 \text{ nm}$) radii and h_{d1} ($= 2 \text{ nm}$) and h_{d2} ($= 3 \text{ nm}$) heights, for QD1 and QD2, respectively. The MNP is a sphere with a radius r_m ($= 8 \text{ nm}$), the distance between the DQDs and the MNP is denoted by R ($= 7 \text{ nm}$); see Fig. 1. A Coulombic study assumes strong coupling; of course, $R < r_m < r_{d1}$ and r_{d2} must be fulfilled [17] as strong coupling conditions. The dielectric constants ε_s and ε_M are defined as those of the QD and MNP, respectively. WL is the QW on which the QDs are grown.

3 Theoretical model

3.1 Wave function

The QD wavefunction is defined in cylindrical coordinates (ρ, ϕ, z) as follows [9],

$$\varphi_{QD}(\vec{r}) = \varphi_d(\vec{\rho})\varphi_{QD}(\vec{z})u(\vec{r}) \quad (1)$$

The in-plane QD envelope function $\varphi_d(\vec{\rho})$ is defined by $J_m(p\vec{\rho})$, the first kind of Bessel function [9],

$$\varphi_d(\vec{\rho}) = C_{nm} J_m(p\vec{\rho}) \quad (2)$$

where C_{nm} is the normalization constant, and the constant p is defined by,

$$p = \frac{\sqrt{2m_d^*(E_\rho - V_d)}}{\hbar} \quad (3)$$

E_ρ is the QD-energy state in the in-plane direction, and V_d and m_d^* are the potential and the effective mass of the QD, respectively. V_d is taken as zero inside the disk. The QD is defined by the conduction CB (valence VB) band offset $\Delta E_c(\Delta E_v)$. The QD envelope function in the z-direction resembles that of the QW [9],

$$\varphi_{QD}(z) = A_{ZQD} \cos(k_z z) \quad (4)$$

where A_{ZQD} is the normalization constant of the QD function in the z-direction. $u(\vec{r})$ is the periodic part of the Bloch function in the QD crystal. The QW-WL wavefunction is written as [18],

$$\varphi_w(\vec{r}) = \varphi_k^0(\vec{\rho}) \varphi_w(z) u(\vec{r}) \quad (5)$$

where $\varphi_k^0(\vec{\rho})$ is the in-plane ($\vec{\rho}$ -direction) WL wavefunction and the superscript $(^0)$ distinguish it from the orthogonalized wavefunction. It is defined by [18],

$$\varphi_k^0(\vec{\rho}) = A_{w_\rho} \exp(i\vec{k}_{w_\rho} \cdot \vec{\rho}) \quad (6)$$

In the in-plane WL, \vec{k}_{w_ρ} is the wavevector, and A_{w_ρ} is the normalization constant. In the z-direction [18],

$$\varphi_w(z) = A_{w_z} \cos(k_{zw} z) \quad (7)$$

A_{w_z} is the normalization constant, and k_{zw} is the WL wavevector in the z-direction.

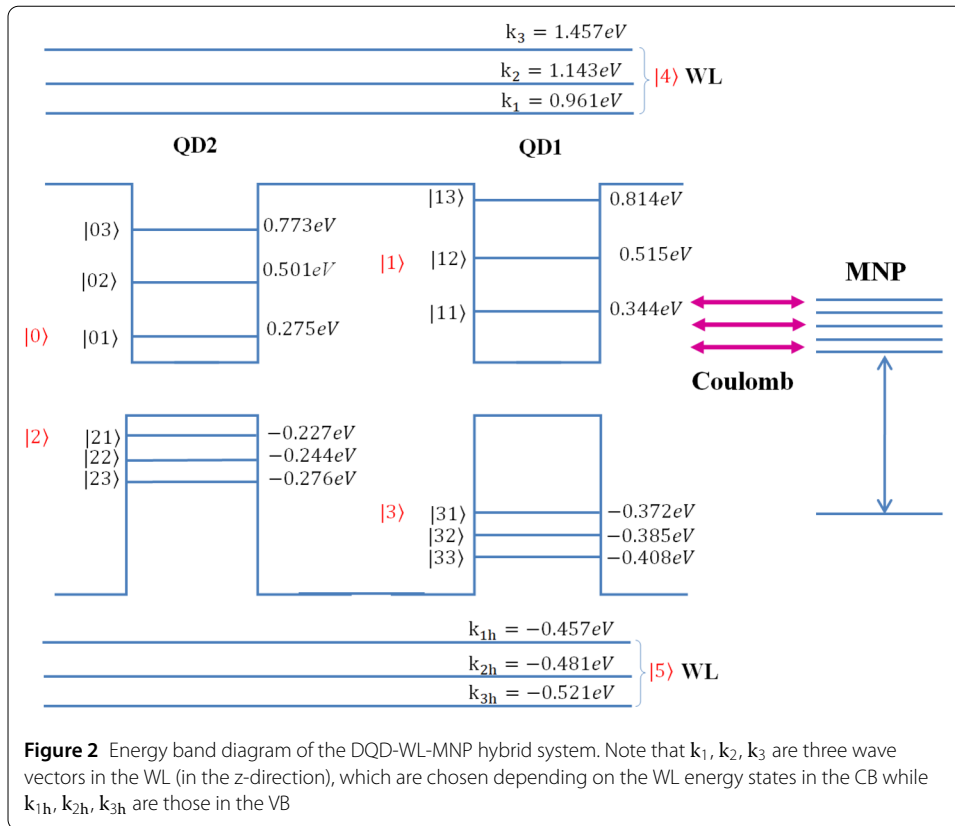
3.2 Coulomb potential

According to [19], the Hamiltonian in the second quantization for carrier–carrier scattering is written for the DQD–WL–MNP hybrid system (Fig. 2) as follows,

$$H_{sys} = H_{kin} + H_C = \sum_b \varepsilon_b a_b^\dagger a_b + V_C(DQD - WL - MNP) \quad (8)$$

The parts define the Hamiltonian H_{kin} as the kinetic contribution and H_C as the Coulomb interaction. The electron creation and annihilation operators are a_x and a_x^\dagger at energy ε_x in the $|x\rangle$ state. The bare Coulomb potential of the DQD-WL-MNP Coulomb interaction is,

$$V_C(DQD - WL - MNP) = \frac{1}{2} \sum_{bfgh} \{ V_{bfgh} a_b^\dagger a_f^\dagger a_g a_h \} + V_M \quad (9)$$



The MNP potential is V_M . Additionally, note that b, f, g , and h in the sum denote all possible electron states. For the QD structure [19, 20],

$$V_{bfg h} = \iint dr dr' \varphi_b^*(r) \varphi_f^*(r') \frac{e_0^2}{4\pi \epsilon_0 \epsilon_{QD} |r - r'|} \varphi_g(r') \varphi_h(r) \quad (10)$$

$\varphi_x(r)$ is the wave function of the single particle. The permittivity of the vacuum and background are given by ϵ_0 and ϵ_{QD} , respectively, and $-e_0$ is the elementary electronic charge. The wave functions are separated into an in-plane \vec{a} -dimensional part and a z-dimensional part. Then, under a Fourier transform, the bare Coulomb potential as a function of the 2D wavevector \vec{q} is [20]

$$V_c(|\vec{r}_1 - \vec{r}_2|) = \sum_q e^{-i\vec{q} \cdot (\vec{\rho} - \vec{\rho}')} V(\vec{q}, z - z') \quad (11)$$

Under [14]

$$V(\vec{q}, \vec{z} - \vec{z}') = \frac{e_0^2}{2\epsilon_0 q} e^{-q|z - z'|} \quad (12)$$

In Eq. (10), the Coulomb potential, including the screening effect (through $\epsilon_0 \epsilon_{QD}$), is defined. Equations (11) and (12) define the bare Coulomb potential. To formulate the problem to the DQD – WL – MNP system under study, with disk shape QDs (in-plane $\vec{\rho}$, and \vec{z} -dimensions quantized) and 2D WL (\vec{z} -dimension quantized only), the bare Coulomb

potential is separated according to the $\vec{\rho}$, and \vec{z} -dimensions dependence wave functions as follows,

$$V_{\nu_2\nu_3\nu_1} = \frac{1}{A} \sum_q V_{\sigma\sigma_2\sigma_3\sigma_1}^{b,b_2}(\vec{q}) \delta_{b,b_1} \delta_{b_2,b_3} \times \langle \varphi_d^b | e^{-i\vec{q}\cdot\vec{\rho}} | \varphi_{k_1}^{b_1} \rangle \langle \varphi_{k_2}^{b_2} | e^{i\vec{q}\cdot\vec{\rho}} | \varphi_{k_3}^{b_3} \rangle \quad (13)$$

A is the WL area, and the available carrier states are $\nu\nu_2\nu_3\nu_1$, while the z-direction quantum numbers are $\sigma, \sigma_2, \sigma_3, \sigma_1$. The DQD states are referred to here by d , while k_i ($i = 1, 2, 3$) refers to the wavevectors in the in-plane direction of the WL. In the 2D-momentum (\vec{q}), the Coulomb potential is given by [19]

$$V_{\sigma\sigma_2\sigma_3\sigma_1}(\vec{q}) = \frac{e_0^2}{2\epsilon_0 q} \iint dz d\hat{z} \varphi_\sigma^*(z) \varphi_{\sigma_2}^*(\hat{z}) e^{-q|z-\hat{z}|} \varphi_{\sigma_1}(z) \varphi_{\sigma_3}(\hat{z}) \quad (14)$$

Considering the approximation [9, 21],

$$|z - \hat{z}| \approx z - \frac{\vec{z}\vec{z}}{z}$$

$$e^{-q|z-\hat{z}|} \approx e^{-q(z-\frac{\vec{z}\vec{z}}{z})}$$

Then, set $q \frac{\vec{z}\vec{z}}{z} \cong \vec{q}$. The Coulomb potential in the z-direction is then written as,

$$V_{\sigma\sigma_2\sigma_3\sigma_1}(\vec{q}) = \frac{e_0^2}{2\epsilon_0 q} \left\{ \left[\int dz \varphi_\sigma^*(z) e^{-qz} \varphi_{\sigma_1}(z) \right] \left[\int d\hat{z} \varphi_{\sigma_2}^*(\hat{z}) e^{q\hat{z}} \varphi_{\sigma_3}(\hat{z}) \right] \right\} \quad (15)$$

3.3 The screened Coulomb matrix element

The screening effect can be introduced through the 2D static limit of the dynamic Lindhard equation [9–11, 19, 22]. In the DQD-WL-MNP hybrid system, the screened Coulomb matrix element is given by

$$W(DQD - WL - MNP)(\vec{q}) = \frac{V_C(DQD - WL - MNP)(\vec{q})}{\epsilon(q)}$$

$$\rightarrow \frac{V_C(DQD - WL - MNP)(\vec{q})}{\frac{1+k_0}{k_{\nu\nu_1}}} \quad (16)$$

The 2D dielectric function $\epsilon(q)$ is defined through the 2D inverse screening length k_0 , given by [10],

$$k_0 = \sum_{b=e,h} \frac{2m_b e^2}{\epsilon_0 \epsilon_{QD} \hbar^2} \left[1 - \exp\left(-\frac{\hbar^2 \pi w_b}{k_B T m_b}\right) \right] \quad (17)$$

The thermal energy is $k_B T$, the effective mass and the frequency of the carrier are m_b and w_b , respectively.

3.4 DQD-MNP applied fields

To calculate Eq. (16), one needs to compute the MNP potential, as shown in Eq. (9). It is estimated from the integration over the DQD-MNP distance R as

$$V_M = - \int_0^R E_{MNP} dR \quad (18a)$$

According to Ref. [23], the DQD-MNP hybrid system has a total field inside the MNP, as shown in Fig. 2, given by,

$$E_{MNP} = \frac{1}{\varepsilon_{effm}} \left[\frac{E_{02}^{(0)}}{2} + \frac{S_a P_{QD}}{\varepsilon_{effs} R^3} \right] \quad (18b)$$

The screening effect is considered for both MNP and DQD fields as [23],

$$\varepsilon_{effi} = \frac{(2\varepsilon_0 + \varepsilon_i)}{3\varepsilon_0} \quad (18c)$$

where ε_i is either ε_s for the dielectric constant of the semiconductor DQD or ε_m for the MNP. The probe amplitude is $E_{02}^{(0)}$, and the polarization in the DQD is $P_{QD} (= \mu_{20}(\rho_{20} + \rho_{02}))$. Considering the probe field applied between QD states (ν, ν_1) , the potential of the MNP reads,

$$V_{M\nu\nu_1} = -\frac{1}{\varepsilon_{effm}} \left[\frac{E_{02}^{(0)}}{2} R - \frac{S_a \mu_{\nu\nu_1} \rho_{\nu\nu_1}}{2\varepsilon_{effs} R^2} \right] \quad (18d)$$

where $\mu_{\nu\nu_1}$ and $\rho_{\nu\nu_1}$ are the momentum and the density matrix elements, respectively, between QD states ν, ν_1 .

The probe field between the states $|0\rangle \leftrightarrow |2\rangle$ of the DQD-MNP system was applied. This field is written as $E_{02}(t) = \frac{E_{02}^{(0)}}{2} e^{-i\omega_{02}t} + \text{c.c.}$ with a transition frequency ω_{02} . Considering the MNP effect, the total QD field is [23],

$$E_{QD} = \frac{1}{2} \frac{E_{02}^{(0)}}{\varepsilon_{effs}} + \frac{S_a P_{MNP}}{\varepsilon_{effs} R^3} \quad (19)$$

The direction of the electric field is specified by S_a , where $S_a = 2$ is the z-axis polarization and $S_a = -1$ is the parallel direction. The MNP-induced polarization is $P_{MNP} (= \beta E_{MNP})$. $\beta (= \gamma a^3)$ defined by [23],

$$\gamma = \frac{\varepsilon_m(\omega) - \varepsilon_0}{\varepsilon_m(\omega) + 2\varepsilon_0} \quad (20)$$

Using the P_{MNP} definition in Eq. (19) and then substituting into Eq. (18b), the total QD field becomes,

$$E_{QD} = \frac{1}{2} \frac{E_{02}^{(0)}}{\varepsilon_{effs}} + \frac{1}{2} \frac{E_{02}^{(0)}}{\varepsilon_{effs}} \frac{S_a \gamma a^3}{R^3} + \frac{S_a^2 \gamma P_{QD}}{\varepsilon_{effs}^2} \frac{a^3}{R^6} \quad (21)$$

The second and third terms in Eq. (21) define the normalized Rabi frequency [16],

$$\Omega_{20}^{(r)} = \Omega_{20}^{(1)} - \eta \rho_{20} \quad (22a)$$

where

$$\Omega_{20}^{(1)} = \Omega_{20}^{(0)} \left(1 + \frac{S_a \gamma a^3}{R^3} \right) \quad (22b)$$

and

$$\eta = \frac{S_a^2 \gamma \mu_{20}^2 a^3}{\hbar \varepsilon_{eff1}^2 R^6} \quad (22c)$$

The definitions in Eq. (22a)–(22c) are attained at strong coupling [16]. Note that the un-normalized Rabi frequency of the probe field is $\Omega_{20}^{(0)} = \frac{\mu_{12} E_{02}^{(0)}}{2\hbar \varepsilon_{effs}}$ [23]. The dielectric function of the MNP is defined by [24],

$$\varepsilon_m(w) = \varepsilon_d(w) + \varepsilon_s(w) \quad (23a)$$

where $\varepsilon_s(w)$ gives the electrons of the s-state contribution to the dielectric constant. It is defined in the Drude model by [24]

$$\varepsilon_s(w) = 1 - \frac{w_p^2}{w^2 + i w (\gamma_{bulk} + \frac{A v_f}{r_m})} \quad (23b)$$

where γ_{bulk} is the damping constant of the metal bulk structure, v_f is the Fermi energy electron velocity, w_p is the metal plasma frequency, A is related to the MNP electron scattering, and $\varepsilon_{IB}(w)$ is the d-state contribution of electrons in the MNP and is defined for the gold-plasma frequency $w_p = 2.5$ (eV) by [24],

$$\varepsilon_d(w) = 1.15 + i10.5 \quad (23c)$$

Using the Drude model to describe electrons in the MNP is a common assumption with a strong coupling regime. Such behavior results from the high electron concentration even with MNP [25–28].

3.5 The processes in the DQD-WL-MNP system under the Coulomb effect

The QD-WL carrier scattering rates are listed in Ref. [11]. For the hybrid DQD-WL-MNP system, shown in Fig. 2, the carrier scattering rate can be written as,

$$S_{b,M,d} = \frac{2\pi}{\hbar} \sum_{k_1, k_2, k_3, b'} [2|W_{M,dk_2k_3k_1}|^2 - W_{M,dk_2k_3k_1} W_{M,dk_3k_2k_1}^*] \delta(\varepsilon_d^b - \varepsilon_{k_1}^b + \varepsilon_{k_2}^{b'} - \varepsilon_{k_3}^{b'}) \times \{(1 - f_d^b) f_{k_1}^b (1 - f_{k_3}^{b'}) f_{k_2}^{b'} - (f \rightarrow 1 - f)\} \quad (24)$$

In Eq. (24), the direct and exchange partners (the first and second terms in the square brackets) determine the screened Coulomb matrix element. The spin degeneracy causes a factor of 2 in the direct Coulomb process. This factor is discarded in the exchange electron-hole process. Accordingly, seven possible scattering processes for the WL-QD-MNP hybrid system are listed in Table 1 (the fifth process is an exchange process added to processes 3 and 4). These processes are diagrammed in Fig. 3.

For the 1st scattering rate in Table 1 (Fig. 3), an electron is captured from the WL electron $|k_1\rangle$ to the $|12\rangle$ electron state in QD₁ with the assistance of the WL transition $|k_2\rangle \rightarrow |k_3\rangle$.

Table 1 QD states where capture and relaxation processes can occur. Note that an assistant process is associated with each process (capture or relaxation) as a four-carrier Coulomb process

No.	Process	Substate
1	Capture Assistant	$ k_1\rangle \rightarrow c_{12}\rangle$ $ k_2\rangle \rightarrow k_3\rangle$
2	Capture Assist	$ k_{1h}\rangle \rightarrow v_{32}\rangle$ $ k_{2h}\rangle \rightarrow k_{3h}\rangle$
3	Relaxation Assist	$ c_{02}\rangle \rightarrow c_{01}\rangle$ $ k_2\rangle \rightarrow k_3\rangle$
4	Relaxation Assist	$ k_2\rangle \rightarrow c_{01}\rangle$ $ c_{11}\rangle \rightarrow k_3\rangle$
5	Coulomb exchange Assist	$ c_{02}\rangle \rightarrow c_{01}\rangle$ $ k_2\rangle \rightarrow k_3\rangle$
6	Mixed Assist	$ k_1\rangle \rightarrow c_{01}\rangle$ $ v_{21}\rangle \rightarrow k_{3h}\rangle$
7	Capture Assist	$ k_1\rangle \rightarrow c_{12}\rangle$ $ c_{01}\rangle \rightarrow c_{11}\rangle$
8	Relaxation Assist	$ c_{02}\rangle \rightarrow c_{01}\rangle$ $ c_{11}\rangle \rightarrow k_1\rangle$

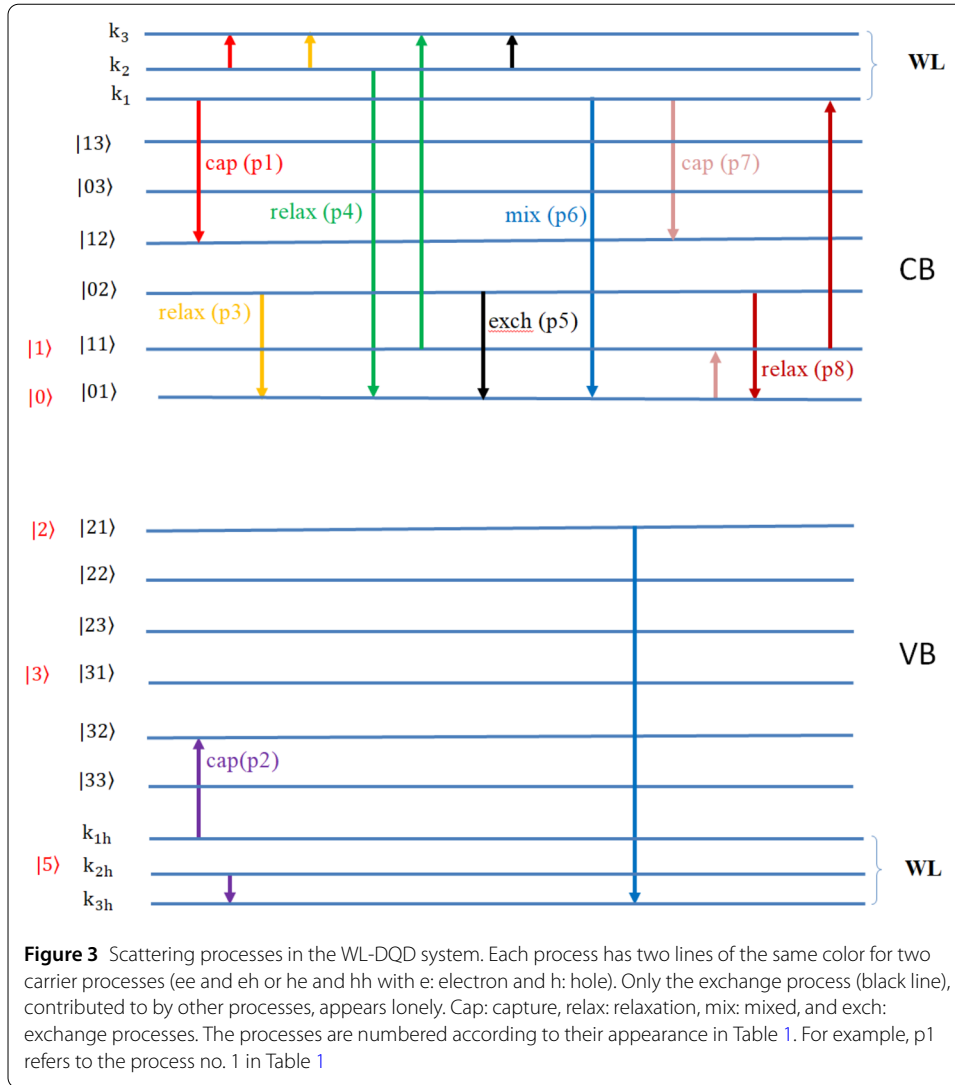
It is written as,

$$\begin{aligned}
 S_{M,e,c_{12}}^{cap} &= S_{M,ee,c_{12}}^{cap} + S_{M,eh,c_{12}}^{cap} \\
 &= \frac{2\pi}{\hbar} \delta(E_{c_{12}}^e - E_{k_1}^e + E_{k_3}^e - E_{k_2}^e) \\
 &\quad \times W_{M,c_{12}k_3k_2k_1} [2W_{M,c_{12}k_3k_2k_1}^* - W_{M,c_{12}k_3k_1k_2}^*] \\
 &\quad \times \{(1-f_{c_{12}})f_{k_1}(1-f_{k_3})f_{k_2} - f_{c_{12}}(1-f_{k_1})f_{k_3}(1-f_{k_2})\} \\
 &\quad + \frac{2\pi}{\hbar} \delta(E_{c_{12}}^e - E_{k_1}^e + E_{k_{3h}}^h - E_{k_{2h}}^h) \times 2|W_{M,c_{12}k_{3h}k_{2h}k_1}|^2 \\
 &\quad \times \{(1-f_{c_{12}})f_{k_1}(1-f_{k_{3h}})f_{k_{2h}} - f_{c_{12}}(1-f_{k_1})f_{k_{3h}}(1-f_{k_{2h}})\}
 \end{aligned} \quad (25)$$

The Coulomb scattering matrix element is $W_{M,c_{12}k_3k_2k_1}$ of the four-carrier DQD interaction under the MNP effect, where M refers to the MNP, c_{12} refers to the $|12\rangle$ QD CB state, and k_i and k_{ih} refer to the WL states according to the quantum numbers in the CB and VB, respectively. $E_{c_{ij}}^e$ is the QD electron energy of the $|ij\rangle$ QD CB state, $E_{k_i}^e$ and $E_{k_{2h}}^h$ are, respectively, that of WL CB electron and VB hole energies corresponding, respectively, to their wave numbers k_i and k_{2h} . f_i refers to the Fermi function of the referred state in the QD or WL in the CB or VB. All these states and wave numbers are clarified in Fig. 2 above. $\delta(E)$ refers to the delta function. The Coulomb matrix element for the e-e interaction is [10],

$$W_{M,c_{12}k_3k_2k_1}(\vec{q}) = \frac{V_{c_{12}k_3k_2k_1}(\vec{q})}{\epsilon(q)} \rightarrow \frac{V_{c_{12}k_3k_2k_1}(\vec{q})}{\frac{1+k_0}{k_{c_{12}}}} \quad (26a)$$

With the $V_{c_{12}k_3k_2k_1}$ is the interaction matrix element of the bare Coulomb potential and $\epsilon(q)$ is the dielectric function. To determine the Coulomb interactions for QD-WL-MNPs,



we have the following integrations:

$$V_{c_{12}k_3k_2k_1} = \{V_{c_{12}k_3k_2k_1}(\vec{z}) \times \langle \Phi_{c_{12}}(\vec{\rho}) | e^{-i\vec{q} \cdot \vec{\rho}} | \Phi_{k_1}(\vec{\rho}) \rangle \langle \Phi_{k_3}(\vec{\rho}) | e^{i\vec{q} \cdot \vec{\rho}} | \Phi_{k_2}(\vec{\rho}) \rangle \} + V_{M02} \quad (26b)$$

In the z-direction, we have

$$V_{c_{12}k_3k_2k_1}(\vec{z}) = \frac{e_0^2}{2\epsilon_0 k_z} \times \langle \Phi_{c_{12}}(\vec{z}) | e^{-\vec{q} \cdot \vec{z}} | \Phi_{k_1}(\vec{z}) \rangle \langle \Phi_{k_3}(\vec{z}) | e^{\vec{q} \cdot \vec{z}} | \Phi_{k_2}(\vec{z}) \rangle \quad (26c)$$

With $\Phi_{c_{ij}}(\vec{\rho})$ and $\Phi_{k_i}(\vec{\rho})$ in Eq. (26b) are, respectively, the in-plane ($\vec{\rho}$) wave functions of the QD and WL in the CB. Also $\Phi_{c_{12}}(\vec{z})$ and $\Phi_{k_1}(\vec{z})$ in Eq. (26c) are their corresponding in the z-direction. V_{M02} is the MNP potential between QD states $|0\rangle$ and $|2\rangle$ where the field is applied. For the WL-DQD system with QDs of a quantum disk shape, it is written (in

the z-direction) as,

$$V_{d_1 k_3 k_2 k_1}(\vec{z}) = \frac{e^2}{2\epsilon_0 k_w} \times \int_0^{z_w} A_{QDz} \cos(k_{zc12} z) \exp(-k_1 z) A_w \cos(k_1 z) dz \\ \times \int_0^{z_w} A_w \cos(\vec{k}_3 \vec{z}) \exp(\vec{k}_2 \vec{z}) A_w \cos(k_2 \vec{z}) d\vec{z} \quad (26d)$$

where k_{zc12} is the QD wavenumber for the QD state, and \vec{k}_3 is the WL wavevector in the QW sublevel, which is slightly different from that represented by k_3 .

3.6 OPW in the QD-WL interaction

In the $\vec{\rho}$ -dimension, some difficulty arises from considering the OPW, which is inevitable in WL-QD transitions. In the $\vec{\rho}$ -dimension, each WL-WL integration has eight integrations due to the consideration of OPW according to [9],

$$\langle \Phi_{k_2} | e^{i\vec{q} \cdot \vec{\rho}} | \Phi_{k_3} \rangle \\ = \frac{1}{N_{k_2} N_{k_3}} \left\{ \langle \Phi_{k_2}^\circ | - \sum_i \langle \Phi_d^i | \langle \Phi_{k_2}^\circ | \Phi_d^i \rangle \right\} e^{i\vec{q} \cdot \vec{\rho}} \left\{ | \Phi_{k_3}^\circ \rangle - \sum_j | \Phi_{d'}^j \rangle \langle \Phi_{d'}^j | \Phi_{k_3}^\circ \rangle \right\} \\ = \frac{1}{N_{k_2} N_{k_3}} \left\{ \langle \Phi_{k_2}^\circ | e^{i\vec{q} \cdot \vec{\rho}} | \Phi_{k_3}^\circ \rangle - \sum_i \langle \Phi_{k_2}^\circ | e^{i\vec{q} \cdot \vec{\rho}} | \Phi_d^i \rangle \langle \Phi_d^i | \Phi_{k_3}^\circ \rangle \right. \\ \left. - \sum_i \langle \Phi_d^i | e^{i\vec{q} \cdot \vec{\rho}} | \Phi_{k_3}^\circ \rangle \langle \Phi_{k_2}^\circ | \Phi_d^i \rangle + \sum_{ij} \langle \Phi_d^i | e^{i\vec{q} \cdot \vec{\rho}} | \Phi_{d'}^j \rangle \langle \Phi_{k_2}^\circ | \Phi_d^i \rangle \langle \Phi_{d'}^j | \Phi_{k_3}^\circ \rangle \right\} \quad (27)$$

with $N_{k_2} = \sqrt{1 - |\sum_i \langle \Phi_d^i | \Phi_{k_2}^\circ \rangle|^2}$. Also, Φ_d^i and $\Phi_{d'}^j$ are the QD wave functions for states $|i\rangle$ and $|j\rangle$ and $\Phi_{k_j}^\circ$ is the WL wave function before using OPW.

3.7 Scattering rates in the WL-DQD-MNP hybrid system

The other scattering rates in the WL-DQD-MNP hybrid system are listed in Table 1 and shown in Fig. 3. Process no. 2 in Table 1 is defined as,

$$S_{M,h,v32}^{cap} = S_{M,h,h,v32}^{cap} + S_{M,h,e,v32}^{cap} \\ = \frac{2\pi}{\hbar} \delta(E_{v32}^h - E_{k_{1h}}^h + E_{k_{3h}}^h - E_{k_{2h}}^h) \\ \times W_{M,v32,k_{3h},k_{2h},k_{1h}} [2W_{M,v32,k_{3h},k_{2h},k_{1h}}^* - W_{M,v32,k_{3h},k_{1h},k_{2h}}^*] \\ \times \{ (1 - f_{v32}) f_{k_{1h}} (1 - f_{k_{3h}}) f_{k_{2h}} - f_{v32} (1 - f_{k_{1h}}) f_{k_{3h}} (1 - f_{k_{2h}}) \} \\ + \frac{2\pi}{\hbar} \delta(E_{v32}^h - E_{k_{1h}}^h + E_{k_3}^e - E_{k_2}^e) \times 2 |W_{M,v32,k_3,k_2,k_{1h}}|^2 \\ \times \{ (1 - f_{v32}) f_{k_{1h}} (1 - f_{k_3}) f_{k_2} - f_{v32} (1 - f_{k_{1h}}) f_{k_3} (1 - f_{k_2}) \} \quad (28)$$

hh and he in the S rates are, respectively, refer to the hole-hole and hole-electron interactions. Please return to Fig. 2 to know the numbering of states in this equation. Process no.

3 in Table 1 is defined as,

$$\begin{aligned}
 S_{M,e,c01}^{relax} &= S_{M,ee,c01}^{relax} + S_{M,eh,c01}^{relax} \\
 &= \frac{2\pi}{\hbar} \times 2 |W_{M,c01k_3k_2c02}|^2 \delta(E_{c01}^e - E_{c02}^e + E_{k_3}^e - E_{k_2}^e) \\
 &\quad \times \{ (1-f_{c01})f_{c02}(1-f_{k_3})f_{k_2} - f_{c01}(1-f_{c02})f_{k_3}(1-f_{k_2}) \} \\
 &\quad + \frac{2\pi}{\hbar} \times 2 |W_{M,c01k_3hk_2hc02}|^2 \delta(E_{c01}^e - E_{c02}^e + E_{k_3h}^h - E_{k_2h}^h) \\
 &\quad \times \{ (1-f_{c01})f_{c02}(1-f_{k_3h})f_{k_2h} - f_{c01}(1-f_{c02})f_{k_3h}(1-f_{k_2h}) \}
 \end{aligned} \tag{29a}$$

Process no. 4 in Table 1 is defined as,

$$\begin{aligned}
 S_{M,e,c01a}^{relax} &= S_{M,ee,c01a}^{relax} + S_{M,eh,c01a}^{relax} \\
 &= \frac{2\pi}{\hbar} \times 2 |W_{M,c01k_3c11k_2}|^2 \delta(E_{c01}^e - E_{k_2}^e + E_{k_3}^e - E_{c11}^e) \\
 &\quad \times \{ (1-f_{c01})f_{k_2}(1-f_{k_3})f_{c11} - f_{c01}(1-f_{k_2})f_{k_3}(1-f_{c11}) \} \\
 &\quad + \frac{2\pi}{\hbar} \times 2 |W_{M,c01k_3hv_31k_2}|^2 \delta(E_{c01}^e - E_{k_2}^e + E_{k_3h}^h - E_{v_31}^h) \\
 &\quad \times \{ (1-f_{c01})f_{k_2}(1-f_{k_3h})f_{v_31} - f_{c01}(1-f_{k_2})f_{k_3h}(1-f_{v_31}) \}
 \end{aligned} \tag{29b}$$

Process no. 5 in Table 1, which is a Coulomb exchange contribution process, is defined as,

$$\begin{aligned}
 S_{M,e,c01b}^{relax} &= S_{M,ee,c01b}^{relax} + S_{M,eh,c01b}^{relax} \\
 &= \frac{2\pi}{\hbar} \times 2 \operatorname{Re} [W_{Mc01k_3k_2c02} W_{Mc01k_3c02k_2}^*] \delta(E_{c01}^e - E_{c02}^e + E_{k_3}^e - E_{k_2}^e) \\
 &\quad \times \{ (1-f_{c01})f_{c02}(1-f_{k_3})f_{k_2} - f_{c01}(1-f_{c02})f_{k_3}(1-f_{k_2}) \} \\
 &\quad + \frac{2\pi}{\hbar} \times 2 \operatorname{Re} [W_{Mc01k_3hk_2hc02} W_{Mc01k_3hc02k_2h}^*] \delta(E_{c01}^e - E_{c02}^e + E_{k_3h}^h - E_{k_2h}^h) \\
 &\quad \times \{ (1-f_{c01})f_{c02}(1-f_{k_3h})f_{k_2h} - f_{c01}(1-f_{c02})f_{k_3h}(1-f_{k_2h}) \}
 \end{aligned} \tag{29c}$$

$\operatorname{Re}()$ refers to the real part. Note that the relaxations in processes 3 and 4 are used with the Coulomb exchange part as follows,

$$S^{relax} = S_{M,e,c01}^{relax} + S_{M,ee,c01a}^{relax} - S_{M,ee,c01b}^{relax} \tag{29d}$$

Additionally, define,

$$S_{M,ee,a}^{relax} = S_{M,ee,c01}^{relax} + S_{M,ee,c01a}^{relax} - S_{M,ee,c01b}^{relax} \tag{29e}$$

$$S_{M,eh,a}^{relax} = S_{M,eh,c01}^{relax} + S_{M,eh,c01a}^{relax} - S_{M,eh,c01b}^{relax} \tag{29f}$$

The subscripts a and b are used to recognize these terms from the above terms that began with the same QD state. Process no. 6 in Table 1 is a mixed process and is defined by

$$S_{M,eh,c_{01}}^{mixed} = \frac{2\pi}{\hbar} \times 2|W_{M,c_{01}k_{3h}v_{21}k_1}|^2 \delta(E_{c_{01}}^e - E_{k_1}^e + E_{k_{3h}}^h - E_{v_{21}}^h) \times \{(1-f_{c_{01}})f_{k_1}(1-f_{k_{3h}})f_{v_{21}} - f_{c_{01}}(1-f_{k_1})f_{k_{3h}}(1-f_{v_{21}})\} \quad (30)$$

Process no. 7 in Table 1 is defined as,

$$\begin{aligned} S_{M,ee,c_{12}}^{cap} &= S_{M,ee,c_{12a}}^{cap} + S_{M,eh,c_{12a}}^{cap} \\ &= \frac{2\pi}{\hbar} \delta(E_{c_{12}}^e - E_{k_1}^e + E_{c_{11}}^e - E_{c_{01}}^e) \\ &\quad \times W_{Mc_{12}c_{11}c_{01}k_1} [2W_{Mc_{12}c_{11}c_{01}k_1}^* - W_{Mc_{12}c_{11}k_1c_{01}}^*] \\ &\quad \times \{(1-f_{c_{12}})f_{k_1}(1-f_{c_{11}})f_{c_{01}} - f_{c_{12}}(1-f_{k_1})f_{c_{11}}(1-f_{c_{01}})\} \\ &\quad + \frac{2\pi}{\hbar} \delta(E_{c_{12}}^e - E_{k_1}^e + E_{v_{31}}^h - E_{v_{21}}^h) \times 2|W_{Mc_{12}v_{31}v_{21}k_1}|^2 \\ &\quad \times \{(1-f_{c_{12}})f_{k_1}(1-f_{v_{31}})f_{v_{21}} - f_{c_{12}}(1-f_{k_1})f_{v_{31}}(1-f_{v_{21}})\} \end{aligned} \quad (31)$$

Process no. 8 in Table 1 is defined as,

$$\begin{aligned} S_{M,b,m}^{relax} &= S_{M,ee,c_{01a}}^{relax} + S_{M,eh,c_{01a}}^{relax} \\ &= \frac{2\pi}{\hbar} \delta(E_{c_{01}}^e - E_{c_{02}}^e + E_{k_1}^e - E_{c_{11}}^e) \\ &\quad \times W_{Mc_{01}k_1c_{11}c_{02}} [2W_{Mc_{01}k_1c_{11}c_{02}}^* - W_{Mc_{01}k_1c_{02}c_{11}}^*] \\ &\quad \times \{(1-f_{c_{01}})f_{c_{02}}(1-f_{k_1})f_{c_{11}} - f_{c_{01}}(1-f_{c_{02}})f_{k_1}(1-f_{c_{11}})\} \\ &\quad + \frac{2\pi}{\hbar} \delta(E_{c_{01}}^e - E_{c_{02}}^e + E_{k_{1h}}^h - E_{v_{31}}^h) \times 2|W_{Mc_{01}k_{1h}v_{31}c_{02}}|^2 \\ &\quad \times \{(1-f_{c_{01}})f_{c_{02}}(1-f_{k_{1h}})f_{v_{31}} - f_{c_{01}}(1-f_{c_{02}})f_{k_{1h}}(1-f_{v_{31}})\} \end{aligned} \quad (32)$$

4 Calculation scenario

Each of the scattering rates of these eight processes in Eqs. (25), (28)-(32) is defined by two types of parameters: the screened Coulomb matrix element W (for direct or exchange process or both) and the Fermi distribution functions $f_{c_{ij}}$ (or $f_{v_{ij}}$). The first type, W , is defined by Eq. (26a) for electrons (and a similar equation for holes), which is calculated through Eq. (26b) and their related integrations in Eqs. (26c), (26d) and the OPW defined in Eq. (27). For the Fermi distribution functions, they are calculated by the distribution functions (ρ_{ii}) for their states ($|0\rangle \dots |5\rangle$), see Fig. 2. The distributions are defined in Appendix B through the density matrix system equations. The first five equations in Appendix B define these distributions as the occupation probabilities of the WL-DQD states. The rest of the equations in Appendix B define the density operators (ρ_{ij}) for the interactions between WL-DQD states ($|i\rangle$ and $|j\rangle$).

The screened Coulomb matrix elements here obey the Markov approximation in the time scale. Thus, the carrier population of the WL-DQD states is cast into the equation $\rho' = S^{in}(1 - \rho) - S^{out}\rho$ [10]. Then, the scattering rates are prepared to this form in Appendix A before introducing them into the density matrix system, Appendix B.

Table 2 The parameters used in the calculations

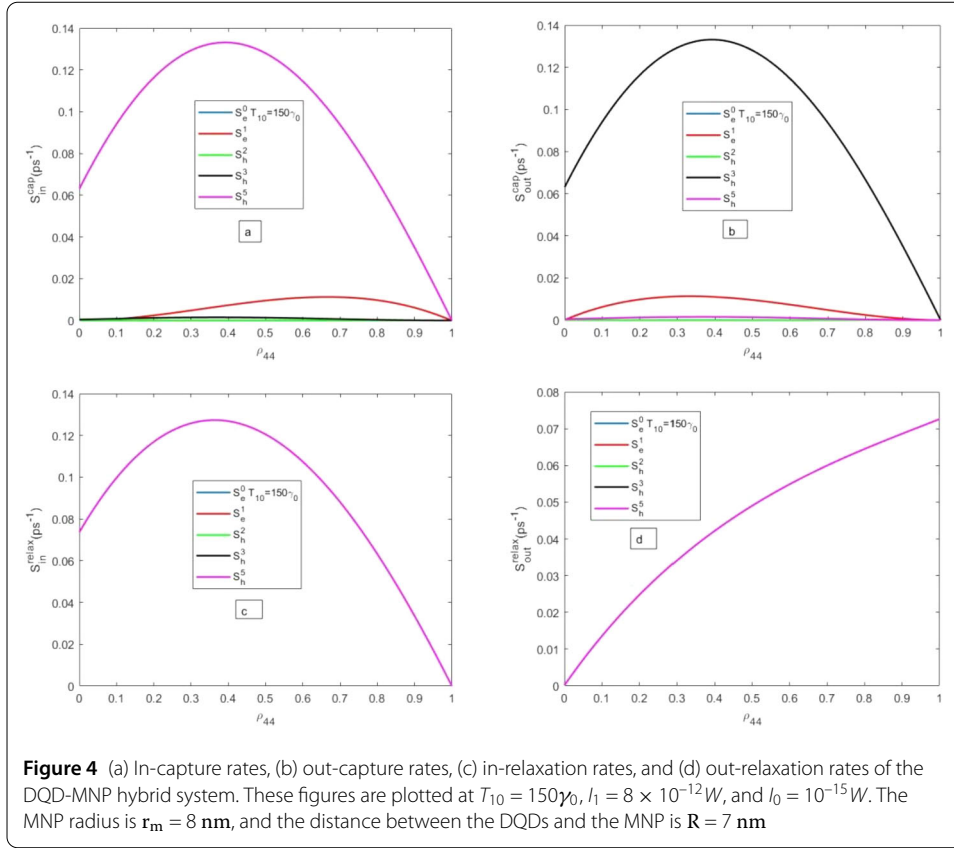
Parameter	Symbol	Value (unit)	Ref.
The Lorentzian line width	$\Gamma (= \gamma_0)$	$1/(2.5 \text{ ns})$	[30]
Dephasing time	τ_f	500 ps	[31]
InAs QD dielectric constant	ϵ_s	$15.15\epsilon_0$	[32]
Damping constant of the bulk metal	γ_{bulk}	0.1 (eV)	[24]
Electron velocity at Fermi energy	v_f	$1.4 \times 10^6 \text{ m/sec}$	[24]
Plasma frequency of the metal	ω_p	2.5 (eV)	[24]
Calculated QD Momenta			
Momentum	Value (nm.e)	Momentum	Value (nm.e)
μ_{10}	13.2789	μ_{25}	4.2353e-05
μ_{20}	4.3492e-04	μ_{35}	4.2667e-05
μ_{03}	0.0014	μ_{14}	6.1838e-04
μ_{32}	2.4485	μ_{04}	6.8385e-04
μ_{31}	6.2797e-04	μ_{21}	3.9315e-04

5 Results and discussion

MAOUD-37 software written in the MATLAB environment [9] was built in our laboratory to interact with the optical properties of QDs, and it is used in many of our articles. Plasmonic structures are also studied by this software [8]. This work involved strong coupling between DQDs and MNPs. It has material properties. The calculations began with QD energy levels, transition momenta, and Rabi frequencies. In the literature, QD energy states and momenta are taken from experimental values for materials different from those under study. This simulation has another property. The Coulomb interaction between QDs and MNPs is considered here, but this interaction is implicitly taken only through the Rabi frequency in the literature. QD energy states are calculated via the quantum disk model [29] and compared with experimental results [8]. The QD-WL-MNP scattering rates are defined in Eqs. (25) and (28)–(32). These equations are introduced to the density matrix system equations in Appendix B, which are then solved via the Runge–Kutta method in the MAOUD-37 software. The resulting energy states and momenta are listed in Table 2 for easy results. The pump and probe powers are defined by $I_i = c\sqrt{\epsilon_b\epsilon_0}|E_i|^2/10^4$, where $i = 0, 1$ is the probe and pump power, and E_i is the intensity. The data used are listed in Table 2.

5.1 DQD-MNPs in the presence of WL (OPW)

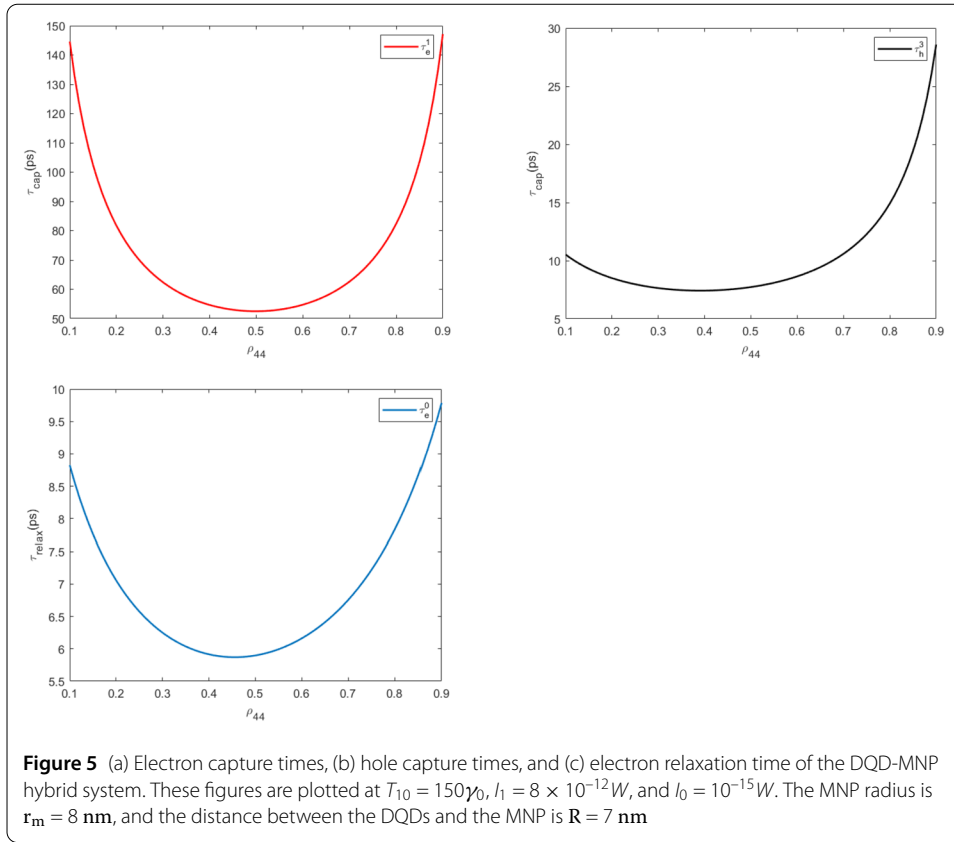
Figure 4 shows the capture and relaxation rates of the WL-DQD-MNP hybrid system. For the in-capture rates, as shown in Fig. 4 (a), the WL hole in-capture rate S_h^5 (magenta curve) is the highest. The peak rate is 0.135 ps^{-1} and occurs at the WL occupation of electrons $\rho_{44} = 0.4$. This result is acceptable because the quantum well WL has many energy states and becomes a carrier reservoir for QDs [33]. As a result, more carriers can enter the WL, and a high carrier scattering rate is obtained. The QD electron rate S_e^1 (the red curve) is less by one order, where its peak is 0.01 ps^{-1} . After that, the QD hole rate S_h^3 appears (the black curve). The QD in-capture rates of S_e^0 and S_h^2 are very low. For the out-capture rate, as shown in Fig. 4 (b), the QD hole rate S_h^3 is the highest, and its peak is 0.135 ps^{-1} . After that, the QD electron rate S_e^1 is 0.01 ps^{-1} . The WL hole rate S_h^5 then appears and is reduced by two orders of magnitude from S_h^3 . The values of S_e^0 and S_h^2 are very small. Figure 4 (c) shows the in-relaxation rates, which are the same for all the states. This is because of the calculation method, which is abstracted in Eqs. (A.2g), (A.2h) in Appendix A below. The



in-relaxation peak occurs at $\rho_{44} \sim 0.4$ and is reduced at complete WL occupation. Figure 4 (d) shows that the out-relaxation rate is one order longer than the in-relaxation rate. Additionally, all the states have the same relaxation for the same reason. The results in Fig. 4 are consistent with those in [34], where the S_h in-and-out-capture rates are the higher rates, having a peak, and the S_h out-rate peaked at 0.12 ps^{-1} . The excited-state in-capture rate for holes is also the highest in [35]. The Pauli blocking is evident in the scattering rate behavior in all panels of Fig. 4, where the rates vanish at complete occupation ($\rho_{44} = 0.4$).

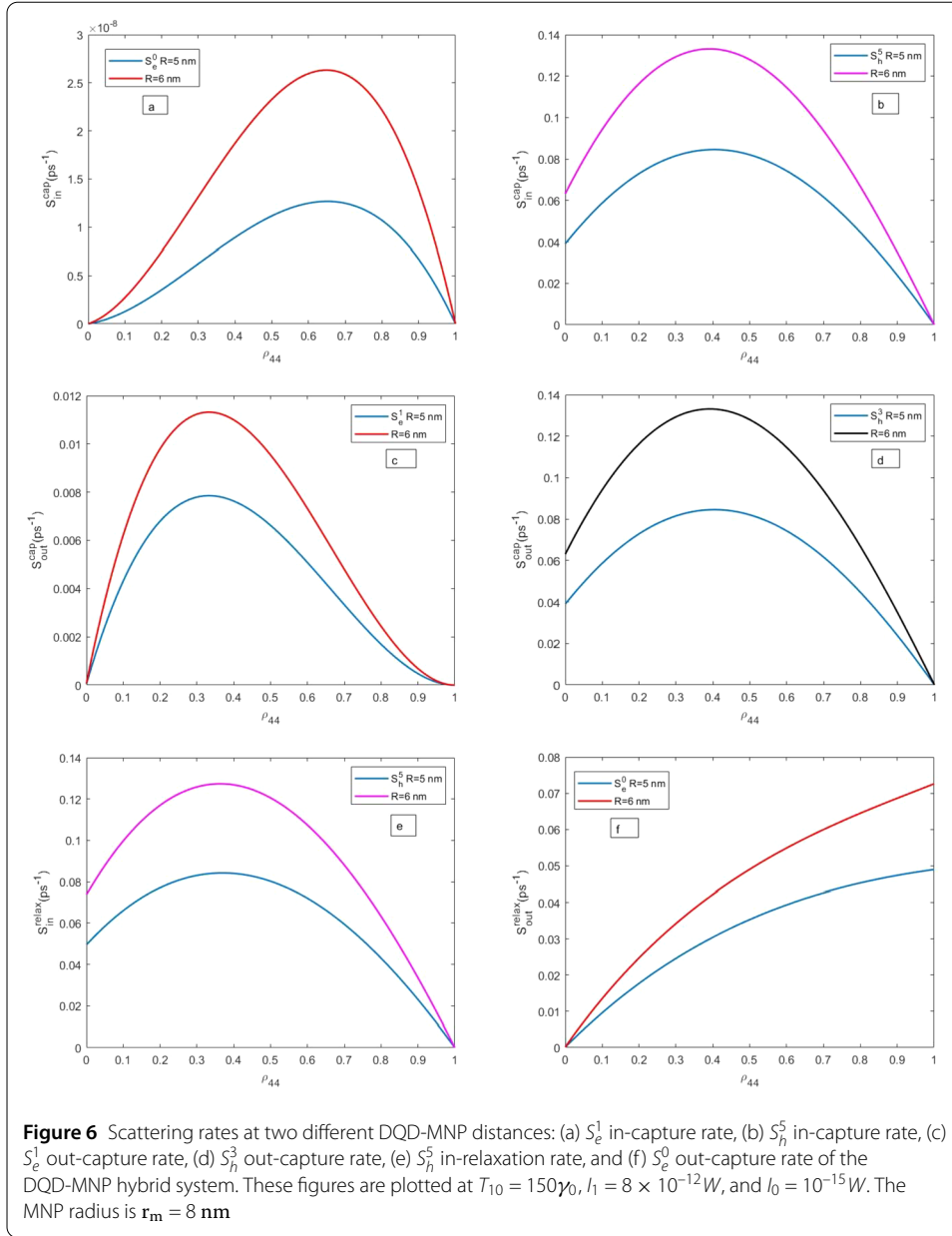
Figure 5 shows the scattering times. Figure 5 (a) illustrates the electron capture time τ_e^1 . Figure 5 (b) shows that the hole capture time τ_h^3 is shorter than the electron capture time in Fig. 5 (a) by one order. This result is with [36]. The electron capture time τ_e is longer than the hole in [11] by more than one order of magnitude. The electron capture time τ_e in [11] is more significant than our results by \sim one order, demonstrating the ability of MNP to shorten the scattering time. The excited-state capture time for holes in [11] doubles our results. Figure 5 (c) shows the relaxation times for electrons and holes, respectively. As the relaxation rates are similar (in relation), their times are identical. At zero and full WL occupation, the relaxation times are high, while a dip occurs at $\rho_{44} \sim 0.45$. The relaxations are less than the hole (electron) capture time by one (two) order(s). The QD relaxation times in [11] are shorter than the capture times, coinciding with our results.

Figure 6 shows the effect of changing the distance R between the DQDs and the MNP on the scattering rate. Figure 6 (a) indicates that the S_e^1 in-capture rate is increased by 0.021 ps^{-1} and peaks at $\rho_{44} = 0.65$ when R is increased by 1 nm . Figure 6 (b) shows that the S_h^5 in-capture rate is increased by 0.04 ps^{-1} , corresponding to a more significant increase



in the hole capture rate. Figure 6 (c) shows that the S_e^1 out capture rate is increased by 0.004 ps^{-1} . Figure 6 (d) shows that the S_h^3 out capture rate increment is 0.05 ps^{-1} . Figure 6 (e) shows that the in-relaxation S_h^5 rate increment is 0.05 ps^{-1} . Figure 6 (f) shows that the out-relaxation rate S_e^0 is 0.02 ps^{-1} at the complete occupation of ρ_{44} . It was shown [37] that QD-MNP properties develop with increasing interparticle distance R . Except for Fig. 6 (f), the scattering rates peak at moderate WL occupation, while the difference between the two curves is maximized at the peak.

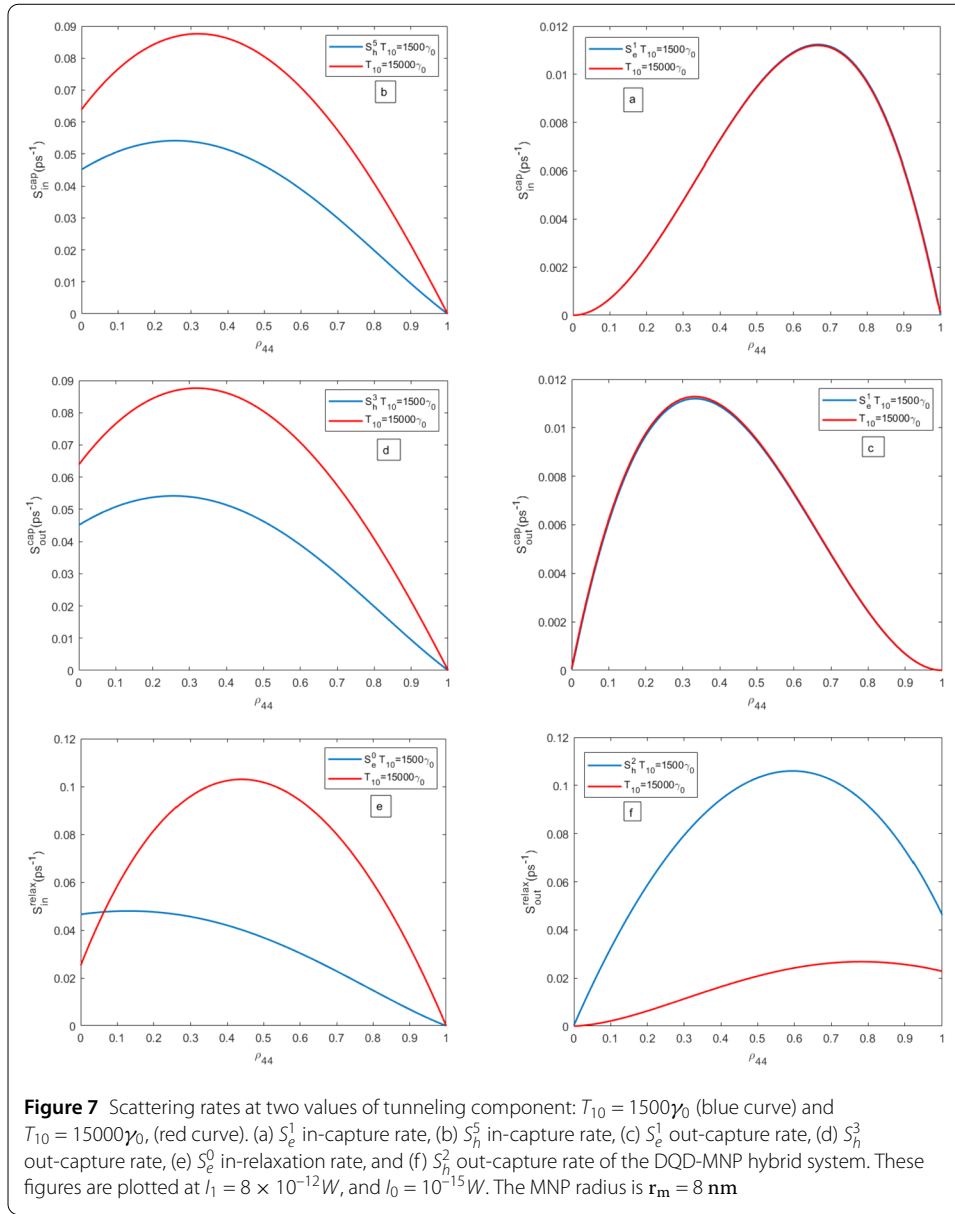
Figure 7 shows the scattering rates at two values of tunneling $T_{10} = 1500\gamma_0$ (blue curve) and $T_{10} = 15,000\gamma_0$, (red curve). The in-and-out-scattering rates with shallow values are not shown here. The S_e^1 in-capture rate, Fig. 7 (a), is not changed under increased tunneling; this is also the case for S_e^1 out-capture rate, Fig. 7 (c). This result occurs due to the vast distance (in energy) between DQD states in the CB, see Fig. 2, and the high relaxation rate from states (greater by one order). So, even high tunneling does not change the situation. The vast energy distance between CB QD states is assigned [29, 38]. The S_h^5 in-capture rate increases under increased tunneling, Fig. 7 (b). When tunneling is increased by one order, S_h^5 in-capture rate is (approximately) doubled. Similar behavior for S_h^3 out-capture rate is shown in Fig. 7 (d). This can be reasoned to the nearest VB QD energy states [29, 38], see Fig. 2. As the relaxations are taken similarly, S_e^0 in-relaxation and S_h^2 out-relaxation rates are shown in Fig. 7 (e) and (f), respectively. It is shown that S_h^2 out-relaxation rate, Fig. 7 (f), is reduced under tunneling; all other scattering rates contradict the behavior. The reason for this is that with increasing tunneling, the carriers can be distributed between DQD



states, and then, there is a possibility of filling new carriers in these states. This behavior means increasing in-relaxation and reducing out-relaxation.

Figure 8 shows the scattering rates at two values of MNP radius. Figure 8 (a) for S_e^1 in-capture rate and Fig. 8 (b) for S_h^3 out-capture rate. In both figures, the change in scattering rate is marginal and occurs at moderate WL electron occupation ρ_{44} . Such behavior occurs because of the strong coupling, and then the system behaves as a whole, and the change under structure parameters is small.

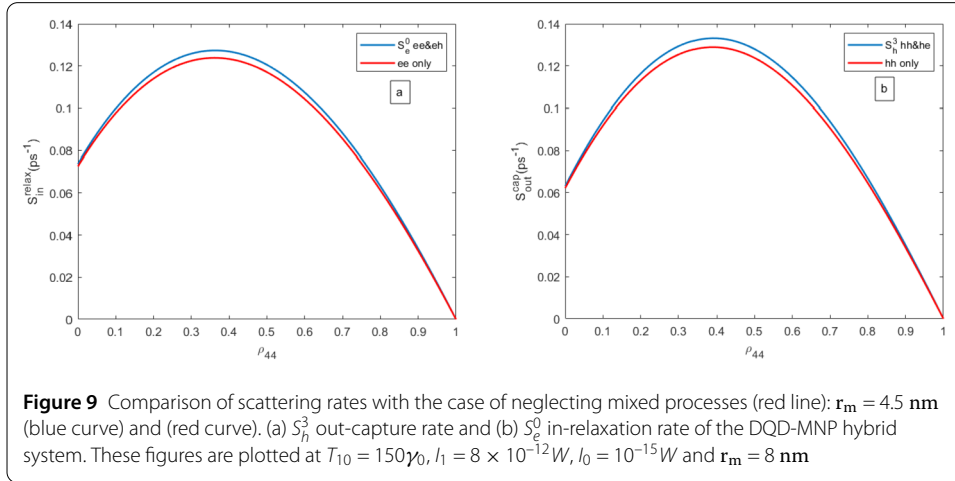
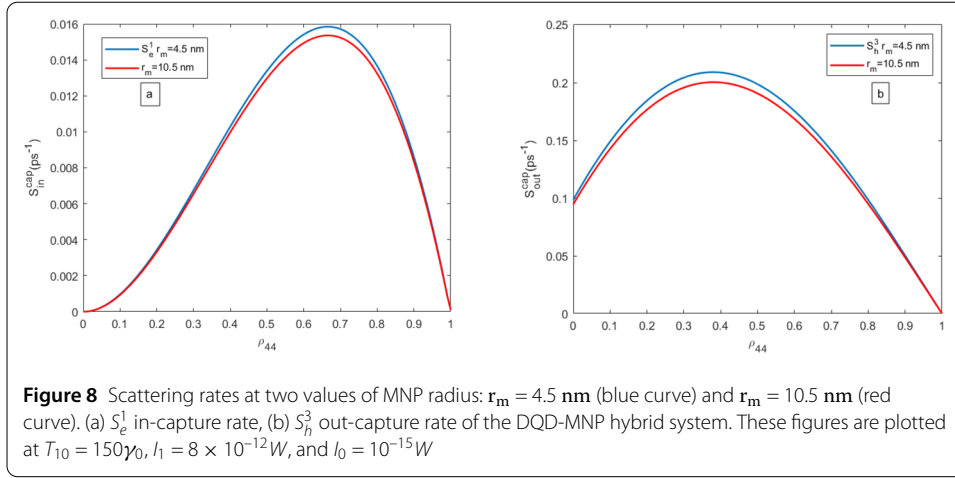
The eh and he (e: electron and h: hole) processes are essential in most of the processes studied here and also to satisfy the stringent energy conservation conditions. Figure 9 shows the scattering rates under the approximation of neglecting these processes to see their importance. The S_e^0 in-capture rate is shown in Fig. 9 (a) and S_h^3 out-capture rate is shown in Fig. 9 (b). Also, the eh and he processes effect is marginal. Such behavior is also



shown in [39]. This work deals with the WL-DQD-MNP hybrid structure under strong coupling. In both Figs. 8 and 9, the marginal change lies under the main effect of the MNP potential.

6 Conclusions

In this work, Coulomb scattering rates in the WL-DQD-MNP structure are modeled considering the MNP potential, which was not modeled earlier. The strong coupling and the OPW are considered. The Rabi frequency is normalized by considering strong coupling. It is then solved in the density matrix theory, where the modeled capture and scattering rates are introduced. The highest capture rate occurs for the QD hole states with the shortest capture times. The electron capture times are more significant than the one-order-of-magnitude relaxation times. The capture rates increase with increasing distance R between the DQDs and the MNP. Tunneling is of great importance in controlling the



scattering rates. From a physical point of view, the scattering rates of the WL-DQD-MNP hybrid structure studied here lie under the Pauli-blocking behavior in filling the states, the energy distance between states, and the effect of the MNP potential under strong coupling.

Appendix A: Capture and relaxation rates

For some DQD states, there is more than one rate (capture or relaxation). Therefore, one needs to introduce the total rate of entering the states. The occupation probability for the states included in the Coulomb matrix element is defined as shown in Eq. (24). Taking the matrix element $W_{M,dk_2k_3k_1}$, the occupations associated with the in-scattering rate are $f_{k_1}^b(1 - f_{k_3}^{b'})f_{k_2}^{b'}$, while those associated with the out-scattering rate are $(1 - f_{k_1}^b)f_{k_3}^{b'}(1 - f_{k_2}^{b'})$. Then, the capture rate that comes from the mixing process in Eq. (30) is written as

$$S_{M,eh,4}^{cap,in} = S_{M,eh,c01}^{mixed} (\rho_{44} \times (1 - \rho_{55}) \times \rho_{22}) \quad (A.1a)$$

$$S_{M,eh,4}^{cap,out} = S_{M,eh,c01}^{mixed} ((1 - \rho_{44}) \times \rho_{55} \times (1 - \rho_{22})) \quad (A.1b)$$

The electron and hole occupation probabilities are ρ_{ii} for the $|i\rangle$ state of the DQD. Note that ρ_{44} and ρ_{55} refer to the WL CB and VB (states $|4\rangle$ and $|5\rangle$) respectively, see Fig. 2. Ad-

ditionally, there are many relaxation processes. The total relaxation rate must be collected. Using Eqs. (29b) and (29c), one can write,

$$S_{M,ee,4}^{rel,in} = S_{M,ee,a}^{relax} (\rho_{00} \times (1 - \rho_{44}) \times \rho_{44}) \quad (\text{A.1c})$$

$$S_{M,ee,4}^{rel,out} = S_{M,ee,a}^{relax} ((1 - \rho_{00}) \times \rho_{44} \times (1 - \rho_{44})) \quad (\text{A.1d})$$

$$S_{M,eh,5}^{rel,in} = S_{M,eh,a}^{relax} (\rho_{00} \times (1 - \rho_{55}) \times \rho_{55}) \quad (\text{A.1e})$$

$$S_{M,eh,5}^{rel,out} = S_{M,eh,a}^{relax} ((1 - \rho_{00}) \times \rho_{55} \times (1 - \rho_{55})) \quad (\text{A.1f})$$

Where $S_{M,ee,4}^{rel,in}$, $S_{M,ee,4}^{rel,out}$, $S_{M,eh,5}^{rel,in}$, $S_{M,eh,5}^{rel,out}$ are the in-and out-scattering relaxation rates for electrons and holes from states $|4\rangle$, $|5\rangle$, respectively. Collecting Eqs. (A.1c) with (A.1e) and (A.1d) with (A.1f) to get,

$$S_{M,e,WD,0}^{rel,in} = S_{M,ee,4}^{rel,in} + S_{M,eh,5}^{rel,in} \quad (\text{A.1g})$$

$$S_{M,e,WD,0}^{rel,out} = S_{M,ee,4}^{rel,out} + S_{M,eh,5}^{rel,out} \quad (\text{A.1h})$$

Where the subscript WD is WL-QD transition. Additionally, there is another relaxation transition. Using Eq. (29b) and (29c),

$$S_{M,ee,1}^{rel,in} = S_{M,ee,a}^{relax} (\rho_{00} \times (1 - \rho_{44}) \times \rho_{11}) \quad (\text{A.2a})$$

$$S_{M,ee,1}^{rel,out} = S_{M,ee,a}^{relax} ((1 - \rho_{00}) \times \rho_{44} \times (1 - \rho_{11})) \quad (\text{A.2b})$$

$$S_{M,eh,3}^{rel,in} = S_{M,eh,a}^{relax} (\rho_{00} \times (1 - \rho_{55}) \times \rho_{33}) \quad (\text{A.2c})$$

$$S_{M,eh,3}^{rel,out} = S_{M,eh,a}^{relax} ((1 - \rho_{00}) \times \rho_{55} \times (1 - \rho_{33})) \quad (\text{A.2d})$$

By combining equations (A.2a) with (A.2b) and (A.2c) with (A.2d), we obtain

$$S_{M,e,DD,0}^{rel,in} = S_{M,ee,1}^{rel,in} + S_{M,eh,3}^{rel,in} \quad (\text{A.2e})$$

$$S_{M,e,DD,0}^{rel,out} = S_{M,ee,1}^{rel,out} + S_{M,eh,3}^{rel,out} \quad (\text{A.2f})$$

Where the subscript DD is for QD-QD transitions. Now, the total relaxation rate is,

$$S_{M,e,0,tot}^{rel,in} = S_{M,e,WD,0}^{rel,in} + S_{M,e,DD,0}^{rel,in} \quad (\text{A.2g})$$

$$S_{M,e,0,tot}^{rel,out} = S_{M,e,WD,0}^{rel,out} + S_{M,e,DD,0}^{rel,out} \quad (\text{A.2h})$$

Where the subscript “tot” refers to the total rate. Also have, for the contributions to the ρ_{11} from Eq. (25),

$$S_{M,ee,c12}^{cap,in} = S_{M,ee,c12}^{cap} (\rho_{44} \times (1 - \rho_{44}) \times \rho_{44}) \quad (\text{A.3a})$$

$$S_{M,ee,c12}^{cap,out} = S_{M,ee,c12}^{cap} ((1 - \rho_{44}) \times \rho_{44} \times (1 - \rho_{44})) \quad (\text{A.3b})$$

$$S_{M,eh,c12}^{cap,in} = S_{M,eh,c12}^{cap} (\rho_{44} \times (1 - \rho_{55}) \times \rho_{55}) \quad (\text{A.3c})$$

$$S_{M,eh,c12}^{cap,out} = S_{M,eh,c12}^{cap} ((1 - \rho_{44}) \times \rho_{55} \times (1 - \rho_{55})) \quad (\text{A.3d})$$

By collecting equations (A.3a) with (A.3c) and (A.3b) with (A.3d), one gets,

$$S_{M,e,W,4}^{cap,in} = S_{M,ee,c_{12}}^{cap,in} + S_{M,eh,c_{12}}^{cap,in} \quad (\text{A.3e})$$

$$S_{M,e,W,4}^{cap,out} = S_{M,ee,c_{12}}^{cap,out} + S_{M,eh,c_{12}}^{cap,out} \quad (\text{A.3f})$$

Additionally, from Eq. (31),

$$S_{M,ee,c_{12a}}^{cap,in} = S_{M,ee,c_{12a}}^{cap} (\rho_{44} \times (1 - \rho_{11}) \times \rho_{00}) \quad (\text{A.4a})$$

$$S_{M,ee,c_{12a}}^{cap,out} = S_{M,ee,c_{12a}}^{cap} ((1 - \rho_{44}) \times \rho_{11} \times (1 - \rho_{00})) \quad (\text{A.4b})$$

$$S_{M,eh,c_{12a}}^{cap,in} = S_{M,eh,c_{12a}}^{cap} (\rho_{44} \times (1 - \rho_{33}) \times \rho_{22}) \quad (\text{A.4c})$$

$$S_{M,eh,c_{12a}}^{cap,out} = S_{M,eh,c_{12a}}^{cap} ((1 - \rho_{44}) \times \rho_{33} \times (1 - \rho_{22})) \quad (\text{A.4d})$$

By collecting Eqs. (A.4a) with (A.4c) and (A.4b) with (A.4d), one gets,

$$S_{M,e,D,4}^{cap,in} = S_{M,ee,c_{12a}}^{cap,in} + S_{M,eh,c_{12a}}^{cap,in} \quad (\text{A.4e})$$

$$S_{M,e,D,4}^{cap,out} = S_{M,ee,c_{12a}}^{cap,out} + S_{M,eh,c_{12a}}^{cap,out} \quad (\text{A.4f})$$

With the total capture rates,

$$S_{M,e,1,tot}^{cap,in} = S_{M,e,W,4}^{cap,in} + S_{M,e,D,4}^{cap,in} \quad (\text{A.4g})$$

$$S_{M,e,1,tot}^{cap,out} = S_{M,e,W,4}^{cap,out} + S_{M,e,D,4}^{cap,out} \quad (\text{A.4h})$$

For ρ_{22}

$$S_{M,e,2}^{cap,in} = S_{M,eh,4}^{cap,out} \quad (\text{A.5a})$$

$$S_{M,e,2}^{cap,out} = S_{M,eh,4}^{cap,in} \quad (\text{A.5b})$$

For ρ_{33} , using Eq. (28),

$$S_{M,hh,v_{32}}^{cap,in} = S_{M,hh,v_{32}}^{cap} (\rho_{55} \times (1 - \rho_{55}) \times \rho_{55}) \quad (\text{A.6a})$$

$$S_{M,hh,v_{32}}^{cap,out} = S_{M,hh,v_{32}}^{cap} ((1 - \rho_{55}) \times \rho_{55} \times (1 - \rho_{55})) \quad (\text{A.6b})$$

$$S_{M,he,v_{32}}^{cap,in} = S_{M,he,v_{32}}^{cap} (\rho_{55} \times (1 - \rho_{44}) \times \rho_{44}) \quad (\text{A.6c})$$

$$S_{M,he,v_{32}}^{cap,out} = S_{M,he,v_{32}}^{cap} ((1 - \rho_{55}) \times \rho_{44} \times (1 - \rho_{44})) \quad (\text{A.6d})$$

Collecting Eqs. (A.6a) with (A.6c) and (A.6b) with (A.6d), one gets,

$$S_{M,e,5,tot}^{cap,in} = S_{M,hh,v_{32}}^{cap,in} + S_{M,he,v_{32}}^{cap,in} \quad (\text{A.6e})$$

$$S_{M,e,5,tot}^{cap,out} = S_{M,hh,v_{32}}^{cap,out} + S_{M,he,v_{32}}^{cap,out} \quad (\text{A.6f})$$

Therefore, for ρ_{33} and ρ_{55}

$$S_{M,e,3}^{cap,in} = S_{M,e,5,tot}^{cap,in} \quad \text{and} \quad S_{M,e,5}^{cap,in} = S_{M,e,5,tot}^{cap,out} \quad (\text{A.6g})$$

$$S_{M,e,3}^{cap,out} = S_{M,e,5,tot}^{cap,out} \quad \text{and} \quad S_{M,e,5}^{cap,out} = S_{M,e,5,tot}^{cap,in} \quad (\text{A.6h})$$

Now, for ρ_{44} in Eqs. (A.1a), (A.1b), (A.3e), (A.3f), and (A.4e), (A.4f),

$$S_{M,e,4,tot}^{cap,in} = S_{M,e,W,4}^{cap,out} + S_{M,eh,4}^{cap,out} + S_{M,e,D,4}^{cap,out} \quad (\text{A.7a})$$

$$S_{M,e,4,tot}^{cap,out} = S_{M,e,W,4}^{cap,in} + S_{M,eh,4}^{cap,in} + S_{M,e,D,4}^{cap,in} \quad (\text{A.7b})$$

Appendix B: Density matrix of the DQD-MNP system under Coulomb scattering with OPW

Applying the density matrix formalism for the WL-DQD-MNP structure, as shown in Fig. 2, under the rotating wave approximation, the change in occupation probability under the probe and pump applied fields with Rabi frequencies Ω_{02} and Ω_{13} and the tunneling component T_{10} with time is written as

$$\begin{aligned} \dot{\rho}_{00} &= S_{M,e,0,tot}^{rel,in} (1 - \rho_{00}) - (S_{M,e,0,tot}^{rel,out} \rho_{00}) + S_{M,eh,4}^{cap,in} (1 - \rho_{00}) - (S_{M,eh,4}^{cap,out} \rho_{00}) \\ &\quad + iT_{10}(\rho_{10} - \rho_{01}) + i(\Omega_{02} - \eta\rho_{20})(\rho_{20} - \rho_{02}) + i\beta_{03}(\rho_{30} - \rho_{03}) + i\beta_{04}(\rho_{40} - \rho_{04}) \\ \dot{\rho}_{11} &= S_{M,e,0,tot}^{rel,in} (1 - \rho_{11}) - (S_{M,e,0,tot}^{rel,out} \rho_{11}) + S_{M,e,1,tot}^{cap,in} (1 - \rho_{11}) - (S_{M,e,1,tot}^{cap,out} \rho_{11}) \\ &\quad + iT_{10}(\rho_{10} - \rho_{01}) + i\beta_{12}(\rho_{21} - \rho_{12}) + i\Omega_{13}(\rho_{31} - \rho_{13}) + i\beta_{14}(\rho_{41} - \rho_{14}) \\ \dot{\rho}_{22} &= S_{M,e,0,tot}^{rel,in} (1 - \rho_{22}) - (S_{M,e,0,tot}^{rel,out} \rho_{22}) - S_{M,e,2}^{cap,in} (1 - \rho_{00}) + (S_{M,e,2}^{cap,out} \rho_{00}) \\ &\quad + i\beta_{23}(\rho_{32} - \rho_{23}) + i(\Omega_{02} - \eta\rho_{20})(\rho_{02} - \rho_{20}) + i\beta_{12}(\rho_{12} - \rho_{21}) + i\beta_{25}(\rho_{52} - \rho_{25}) \\ \dot{\rho}_{33} &= S_{M,e,0,tot}^{rel,in} (1 - \rho_{33}) - (S_{M,e,0,tot}^{rel,out} \rho_{33}) + S_{M,e,3}^{cap,in} (1 - \rho_{33}) - (S_{M,e,3}^{cap,out} \rho_{33}) \\ &\quad + i\beta_{30}(\rho_{03} - \rho_{30}) + i\Omega_{13}(\rho_{13} - \rho_{31}) + i\beta_{23}(\rho_{23} - \rho_{32}) + i\beta_{35}(\rho_{53} - \rho_{35}) \\ \dot{\rho}_{44} &= S_{M,e,0,tot}^{rel,in} (1 - \rho_{44}) - (S_{M,e,0,tot}^{rel,out} \rho_{44}) - S_{M,e,4,tot}^{cap,in} (1 - \rho_{11}) + (S_{M,e,4,tot}^{cap,out} \rho_{11}) \\ &\quad + i\beta_{40}(\rho_{04} - \rho_{40}) + i\beta_{41}(\rho_{14} - \rho_{41}) \\ \dot{\rho}_{55} &= S_{M,e,0,tot}^{rel,in} (1 - \rho_{55}) - (S_{M,e,0,tot}^{rel,out} \rho_{55}) - S_{M,e,5}^{cap,in} (1 - \rho_{33}) + (S_{M,e,5}^{cap,out} \rho_{33}) \\ &\quad + i\beta_{52}(\rho_{25} - \rho_{52}) + i\beta_{53}(\rho_{35} - \rho_{53}) \\ \dot{\rho}_{10} &= -(\gamma_0 + \gamma_1)\rho_{10} + iT_{10}(\rho_{00} - \rho_{11}) + (i\beta_{12}\rho_{20}) + (i\Omega_{13}\rho_{30}) + (i\beta_{14}\rho_{40}) \\ &\quad - i(\Omega_{02} - \eta\rho_{20})\rho_{12} - i\beta_{30}\rho_{13} - i\beta_{40}\rho_{14} \\ \dot{\rho}_{20} &= (\rho_{20}(-i\Delta_{20}) - (\gamma_0 + \gamma_2)) + i(\Omega_{20} - \eta\rho_{20})(\rho_{00} - \rho_{22}) + (i\beta_{21}\rho_{10}) + i\beta_{23}\rho_{30} \\ &\quad - (i\beta_{40}\rho_{24}) - iT_{10}\rho_{21} - (i\beta_{30}\rho_{23}) - i\beta_{52}\rho_{25} \\ \dot{\rho}_{30} &= -(\gamma_0 + \gamma_3)\rho_{30} + i\beta_{30}(\rho_{00} - \rho_{33}) + (i\beta_{13}\rho_{10}) + i\beta_{23}\rho_{20} \\ &\quad - iT_{10}\rho_{31} - i(\Omega_{20} - \eta\rho_{20})\rho_{32} + (i\beta_{35}\rho_{50}) - (i\beta_{40}\rho_{34}) \\ \dot{\rho}_{40} &= -(\gamma_0 + \gamma_4)\rho_{40} - i(\Omega_{20} - \eta\rho_{20})\rho_{42} + i\beta_{40}(\rho_{00} - \rho_{44}) + (i\beta_{41}\rho_{10}) - iT_{10}\rho_{14} - (i\beta_{30}\rho_{43}) \\ \dot{\rho}_{21} &= -(\gamma_2 + \gamma_1)\rho_{21} + i\beta_{21}(\rho_{11} - \rho_{22}) + i(\Omega_{20} - \eta\rho_{20})\rho_{01} + i\beta_{23}\rho_{31} + (i\beta_{25}\rho_{51}) \\ &\quad - iT_{10}\rho_{20} - (i\beta_{41}\rho_{24}) - (i\Omega_{13}\rho_{23}) \end{aligned}$$

$$\begin{aligned}
\dot{\rho}_{31} &= -(\gamma_3 + \gamma_1)\rho_{31} + i\Omega_{13}(\rho_{11} - \rho_{33}) + (i\beta_{30}\rho_{01}) + i\beta_{23}\rho_{21} \\
&\quad - iT_{10}\rho_{30} - (i\beta_{21}\rho_{32}) + (i\beta_{35}\rho_{51}) - (i\beta_{41}\rho_{34}) \\
\dot{\rho}_{41} &= -(\gamma_4 + \gamma_1)\rho_{41} + i\beta_{41}(\rho_{11} - \rho_{44}) + (i\beta_{40}\rho_{01}) - iT_{10}\rho_{40} - (i\beta_{21}\rho_{42}) - (i\Omega_{13}\rho_{43}) \\
\dot{\rho}_{23} &= -(\gamma_2 + \gamma_3)\rho_{23} + i\beta_{23}(\rho_{33} - \rho_{22}) + i(\Omega_{20} - \eta\rho_{20})\rho_{03} - i\beta_{53}\rho_{25} + (i\beta_{21}\rho_{13}) \\
&\quad + (i\beta_{25}\rho_{53}) - (i\beta_{03}\rho_{20}) - (i\beta_{53}\rho_{25}) - (i\Omega_{13}\rho_{21}) \\
\dot{\rho}_{24} &= -(\gamma_2 + \gamma_4)\rho_{42} + i(\Omega_{20} - \eta\rho_{20})\rho_{04} + i\beta_{21}\rho_{41} - (i\beta_{14}\rho_{21}) - (i\beta_{04}\rho_{20}) + i\beta_{23}\rho_{34} \\
\dot{\rho}_{25} &= -(\gamma_2 + \gamma_5)\rho_{25} + i(\Omega_{20} - \eta\rho_{20})\rho_{05} + i\beta_{25}(\rho_{55} - \rho_{22}) \\
&\quad + i\beta_{23}\rho_{25} - (i\beta_{35}\rho_{23}) + (i\beta_{21}\rho_{15}) \\
\dot{\rho}_{35} &= -(\gamma_3 + \gamma_5)\rho_{35} + i\beta_{23}\rho_{25} + i\beta_{35}(\rho_{55} - \rho_{33}) + (i\beta_{30}\rho_{05}) + (i\beta_{31}\rho_{15}) - (i\beta_{25}\rho_{32}) \\
\dot{\rho}_{43} &= -(\gamma_4 + \gamma_3)\rho_{43} + i\beta_{40}\rho_{03} + (i\beta_{41}\rho_{13}) - (i\beta_{03}\rho_{40}) - (i\Omega_{13}\rho_{41}) - i\beta_{23}\rho_{42} \\
\dot{\rho}_{50} &= -(\gamma_5 + \gamma_0)\rho_{50} + i\beta_{52}\rho_{20} + (i\beta_{53}\rho_{30}) - iT_{10}\rho_{50} - i(\Omega_{20} - \eta\rho_{20})\rho_{52} - (i\beta_{30}\rho_{53}) \\
\dot{\rho}_{51} &= -(\gamma_5 + \gamma_1)\rho_{51} + i\beta_{52}\rho_{21} + (i\beta_{53}\rho_{31}) - iT_{10}\rho_{50} - (i\beta_{21}\rho_{52}) - (i\Omega_{13}\rho_{53}) \quad (B.1)
\end{aligned}$$

The electron and hole occupation probabilities are ρ_{ii} for the $|i\rangle$ state of the DQD, while the density operator ρ_{ij} defines the interaction between DQD states $|i\rangle$ and $|j\rangle$. $\beta_{ij} = \frac{A_{ij}}{2} + \frac{1}{\tau_t}$, where $A_{ij} (= \frac{\mu_{ij}^2 \omega_{ij}^2}{3\pi \hbar \epsilon_s c^3})$ is the Einstein coefficient, τ_t is the dipole dephasing time, and ω_{ij} is the transition frequency between the $|i\rangle$ and $|j\rangle$ states in the WL-DQD structure. The momentum of the transitions between the WL-QD and QD-QD transitions is μ_{ij} . The momentum calculations are defined well in [16]. Based on the calculated momenta, the normalized Rabi frequency is computed from Eq. (22a)–(22c). Then, β_{ij} is calculated depending on the computed momenta values.

Funding

The authors declare no funding.

Data Availability

No datasets were generated or analysed during the current study.

Declarations

Ethics approval and consent to participate

The work was not sent to any other site. All the authors consented to participate.

Consent for publication

All the authors consent to publication.

Competing interests

The authors declare no competing interests.

Author contributions

All authors are contributed equally.

Received: 31 January 2024 Accepted: 13 March 2024 Published online: 26 March 2024

References

- Ramirez HY. Double dressing and manipulation of the photonic density of states in nanostructured qubits. *RSC Adv.* 2013;3:24991–6.
- Trügler A, Hohenester U. Strong coupling between a metallic nanoparticle and a single molecule. *Phys Rev B.* 2008;77:115403.
- Artuso RD, Bryant GW. Strongly coupled quantum dot-metal nanoparticle systems: exciton-induced transparency, discontinuous response, and suppression as driven quantum oscillator effects. *Phys Rev B.* 2010;82:195419.

4. Artuso RD, Bryant GW. Optical response of strongly coupled quantum dot-metal nanoparticle systems: double peaked Fano structure and bistability. *Nano Lett.* 2008;8:2106–11.
5. He Y, Zhu K-D. Fano correlation effect of optical response due to plasmon–exciton–plasmon interaction in an artificial hybrid molecule system. *J Opt Soc Am B.* 2013;30:868–73.
6. Hohenester U, Trugler A. Interaction of single molecules with metallic nanoparticles. *IEEE J Sel Top Quantum Electron.* 2008;14:1430–40.
7. Lingnau B, Lüdge K, Schöll E, Chow WW. Many-body and nonequilibrium effects on relaxation oscillations in a quantum-dot microcavity laser. *Appl Phys Lett.* 2010;97:111102.
8. Akram H, Abdullah M, Al-Khursan AH. Energy absorbed from double quantum dot-metal nanoparticle hybrid system. *Sci Rep.* 2022;12:21495.
9. Abbas MAA, Al-Badry LF, Al-Khursan AH. Coulomb effect in double quantum dot system. *J Electron Mater.* 2022;51:1202–14.
10. Malic E, Bormann MJP, Hovel P, Kuntz M, Bimberg D, Knorr A, Scholl E. Coulomb damped relaxation oscillations in semiconductor quantum dot lasers. *IEEE J Sel Top Quantum Electron.* 2007;13:1242–8.
11. Nielsen TR, Gartner P, Jahnke F. Many-body theory of carrier capture and relaxation in semiconductor quantum-dot lasers. *Phys Rev B.* 2004;69:235314.
12. Tarasov GG, Zhuchenko YZ, Lisitsa MP, Mazur YI, Wang ZM, Salamo GJ, Warming T, Bimberg D, Kissel H. Optical detection of asymmetric quantum-dot molecules in double-layer InAs/GaAs structures. *Semiconductors.* 2006;40:79–83.
13. Richardson HH, Carlson MT, Tandler PJ, Hernandez P, Govorov AO. Experimental and theoretical studies of light-to-heat conversion and collective heating effects in metal nanoparticle solutions. *Nano Lett.* 2009;9:1139–46.
14. Zhang W, Govorov AO, Bryant GW. Semiconductor-metal nanoparticle molecules: hybrid excitons and the nonlinear Fano effect. *Phys Rev Lett.* 2006;97:146804.
15. Zhang Y, Eyink K, Urwin B, Mahalingam K, Hill M. A self-assembling method to align metal nanoparticles to quantum dots. *J Cryst Growth.* 2023;605:127072.
16. Hameed AH, Al-Khursan AH. Tunability of plasmonic electromagnetically induced transparency from double quantum dot-metal nanoparticle structure under transition momenta. *Opt Quantum Electron.* 2023;55:1213.
17. Yan JY, Zhang W, Duan S, Zhao XG, Govorov AO. Optical properties of coupled metal-semiconductor and metal-molecule nanocrystal complexes: role of multipole effects. *Phys Rev B.* 2008;77:165301.
18. Asada M, Kameyama A, Suematsu Y. Gain and intervalence band absorption in quantum well lasers. *IEEE J Quantum Electron.* 1984;QE-20:745–53.
19. Lingnau B. Nonlinear and nonequilibrium dynamics of quantum dot optoelectronic devices. PhD Thesis, TU-Berlin-Germany, Springer thesis. 2015.
20. Magnusdottir I, Bischoff S, Uskov AV, Mørk J. Geometry dependence of Auger carrier capture rates into cone-shaped self-assembled quantum dots. *Phys Rev B.* 2003;67:205326.
21. Davidov AS. *Quantum mechanics*. 2nd ed. Oxford: Pergamon; 1965.
22. Chow WW, Koch SW. *Semiconductor-laser: fundamentals physics of the gain materials*. New York: Springer; 1990.
23. Sadeghi SM, Deng L, Li X, Huang WP. Plasmonic (thermal) electromagnetically induced transparency in metallic nanoparticle–quantum dot hybrid systems. *Nanotechnology.* 2009;20:365401.
24. Hatef A, Sadeghi SM, Singh MR. Plasmonic electromagnetically induced transparency in metallic nanoparticle–quantum dot hybrid systems. *Nanotechnology.* 2012;23:065701.
25. Waks E, Sridharan D. Cavity QED treatment of interactions between a metal nanoparticle and a dipole emitter. *Phys Rev A* 2010;82:043845.
26. Hakami J, Suhail Zubairy M. Nanoshell-mediated robust entanglement between coupled quantum dots. *Phys Rev A.* 2016;93:022320.
27. Alpeggiani F, D'Agostino S, Claudio Andreani L. Surface plasmons and strong light-matter coupling in metallic nanoshells. *Phys Rev B.* 2012;86:035421.
28. Hakami J, Wang L, Suhail Zubairy M. Spectral properties of a strongly coupled quantum-dot–metal-nanoparticle system. *Phys Rev A.* 2014;89:053835.
29. Kim J, Chuang SL. Theoretical and experimental study of optical gain, refractive index change, and line width enhancement factor of p-doped quantum-dot lasers. *IEEE J Quantum Electron.* 2006;42:942–52.
30. Gioannini M, Montrosset I. Numerical analysis of the frequency chirp in quantum-dot semiconductor lasers. *IEEE J Quantum Electron.* 2007;43:941–9.
31. Sridharan D, Waks E. All-optical switch using quantum-dot saturable absorbers in a DBR microcavity. *IEEE J Quantum Electron.* 2011;47:31–9.
32. Chuang SL. *Physics of optoelectronic devices*. New York: Wiley; 1995.
33. Xiao JL, Huang YZ. Numerical analysis of gain saturation, noise figure, and carrier distribution for quantum-dot semiconductor-optical amplifiers. *IEEE J Quantum Electron.* 2008;44:448–55.
34. Wegert M, Majer N, Lüdge K, Volkel SD, Bresco JG, Knorr A, Woggon U, Scholl E. Nonlinear gain dynamics of quantum dot optical amplifiers. *Semicond Sci Technol.* 2011;26:014008.
35. Majer N, Lüdge K, Schöll E. Cascading enables ultrafast gain recovery dynamics of quantum dot semiconductor optical amplifiers. *Phys Rev B.* 2010;82:235301.
36. Lüdge K, Schöll E. Temperature dependent two-state lasing in quantum dot lasers. In: 2011 fifth Rio de la Plata workshop on laser dynamics and nonlinear photonics, Colonia del Sacramento, Uruguay; 2011. p. 1–6. <https://doi.org/10.1109/LDNP.2011.6162081>.
37. Kosionis SG, Terzis AF, Sadeghi SM, Paspalakis E. Optical response of a quantum dot–metal nanoparticle hybrid interacting with a weak probe field. *J Phys Condens Matter.* 2013;25:045304.
38. Kim J, Laemmlin M, Meuer C, Bimberg D, Eisenstein G. Static gain saturation model of quantum-dot semiconductor optical amplifiers. *IEEE J Quantum Electron.* 2008;44:658–66.

39. Lüdge K, Bormann MJP, Malić E, Hövel P, Kuntz M, Bimberg D, Knorr A, Schöll E. Turn-on dynamics and modulation response in semiconductor quantum dot lasers. *Phys Rev B*. 2008;78:035316.

Publisher's Note

Springer Nature remains neutral with regard to jurisdictional claims in published maps and institutional affiliations.

Submit your manuscript to a SpringerOpen[®] journal and benefit from:

- Convenient online submission
- Rigorous peer review
- Open access: articles freely available online
- High visibility within the field
- Retaining the copyright to your article

Submit your next manuscript at ► [springeropen.com](https://www.springeropen.com)
